World Academy of Science, Engineering and Technology
International Journal of Computer and Information Engineering
Vol:8, No:8, 2014

Magnet Position Variation of the Electromagnetic Actuation System in a Torsional Scanner

Loke Kean Koay, Mani Maran Ratnam

***Abstract*—**A mechanically-resonant torsional spring scanner was developed in a recent study. Various methods were developed to improve the angular displacement of the scanner while maintaining the scanner frequency. However the effects of rotor magnet radial position on scanner characteristics were not well investigated. In this study, the relationships between the magnet position and the scanner characteristics such as natural frequency, angular displacement and stress level were studied. A finite element model was created and an average deviation of 3.18% was found between the simulation and experimental results, qualifying the simulation results as a guide for further investigations. Three magnet positions on the transverse oscillating suspended plate were investigated by finite element analysis (FEA) and one of the positions were selected as the design position. The magnet position with the longest distance from the twist axis of mirror was selected since it attains minimum stress level, while exceeding the minimum critical flicker frequency and delivering the targeted angular displacement to the scanner.

***Keywords*—**Computer-aided design, design optimization, torsional scanner.

I. Introduction

TORSIONAL scanners play a central role in many systems such as high-energy laser systems (HEL) [1], free-space optical communications [2], semiconductor manufacturing and inspection, laser welding, laser cutting of materials [3], optical data storage, information display [4], scanning optical lithography [1] and various applications in medical and biomedical systems [5]–[7].

Generally, torsional scanners can be categorized into two groups, one with a rotatable frame and the other with a rotatable mirror. The rotatable frame system consists of a light source (laser) which generally has a larger inertia mounted on gimbals driven by actuators [8]. Meanwhile, the rotatable mirror system consists of a light-weight oscillating mirror. The light source is reflected from the moving mirror resulting in a scanned output light without the need for large moving mass [8]. The rotatable mirror has the advantages of lower inertia and faster response, which greatly increases the bandwidth of the operation compared to the rotatable frame technique.

Various actuators have been designed to actuate the mirror in a torsional scanner. They typically consist of a galvanometer, a piezoelectric actuator or a voice-coil motor (VCM) [2]. Most modern galvanometer positioning actuators work on permanent magnet motor principles. The galvanometer makes use of the interaction between a permanent magnet and the magnetic field created by a current in a wire coil resulting in a rotary torque on the actuator's rotor which is suspended on a set of bearings [9]. However, galvanometer scanners suffer from disadvantages such as large size, high power consumption, and nonlinear distortion caused by the rotational inertia during fast linear scanning (scanning at uniform scanning line velocity with high frequency) [2], [5].

Piezoelectric actuators are electro-mechanical transducers that transform electrical energy into mechanical motion via the inverse piezoelectric effect. The piezoelectric effect is employed in actuators that produce small displacements with extremely fine resolution (sub-nanometer) or over small travel ranges (several micrometers); the travel range is limited by the dielectric strength and the thickness of the piezoelectric material [10], [11]. Torsional scanners driven by the piezoelectric effect usually have high resonant frequencies but they cannot offer large deflection angles.

The structure of VCM can be understood by the components used in traditional electrodynamics loudspeakers, consisting of permanent magnet and a coil linked by a compliant structure. The presence of an iron core in the VCM's coil will lead to several kinds of nonlinearities. These include Eddy currents, magnetic saturation of the iron and the variation of the coil inductance with its position causing a reluctant force effect [12]. These drawbacks can be overcome by using air-core coils that have no hysteresis due to the absence of ferromagnetic materials, no eddy current loss and no flux saturation [13]. The VCM can deliver large deflection angles and reasonably high frequency; therefore it was selected as the actuator in this study.

In a previous study [14], a mechanically-resonant torsional spring scanner was designed based on a rotatable mirror and VCM system. The mechanically-resonant torsional spring scanner shown in Fig. 1 consists of a mirror (2) and a suspended plate (3) mounted on a torsional spring (5). A laser pointer (1) is aimed at the mirror (2). The magnet (7) attached to the suspended plate (3) is attracted or repelled by the air-core coil (4) causing angular deflection of the mirror. When excited at the resonant frequency, the suspended plate and the mirror are able to oscillate at large amplitudes with low power consumption [15]. The angular displacement of the mirror depends on the Q-factor of vibration, dampening, the position of magnet attached onto the suspended plate, the current through the coil and, hence, the magnetic flux in the coil area. According to Urey [4], to obtain a high Q-factor it is desirable

Loke Kean Koay is with the Mechanical Section, Malaysian Spanish Institution, Universiti Kuala Lumpur, Kulim Hi-tech Park, 09000 Kulim, Kedah, Malaysia (corresponding author to provide phone: +6016-4340182; e-mail: lkean85@hotmail.com).

Mani Maran Ratnam is with School of Mechanical Engineering, Engineering Campus, Universiti Sains Malaysia, 14300, NibongTebal, Penang, Malaysia (e-mail: mmaran@eng.usm.my).

to use the torsional mode as the first mode, i.e. mode with the lowest frequency.

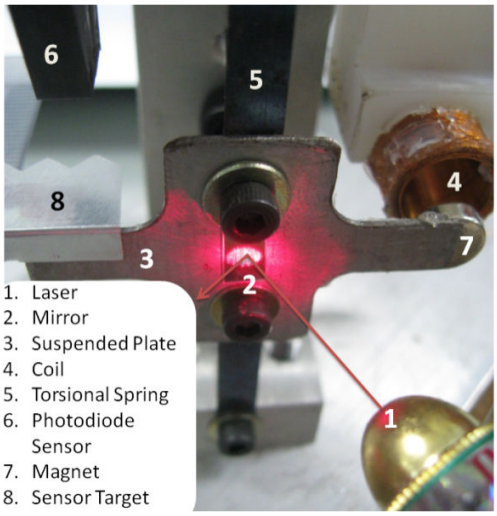

Fig. 1 Torsional spring and device components

The challenge in the mechanical design of the mechanically-resonant torsional spring scanner is to find a compromise between contradictory requirements of the various characteristics of the scanner. The main characteristics include the angular displacement, resonant frequency, stress level, shock overload, mirror flatness, current, power and cost. The resonant frequency of the system must be kept above the Critical Flickering Frequency (CFF). The CFF is the minimum frequency required to avoid perceptible flickering of the scanned image [16]–[18]. To increase the scanner's resonant frequency, the stiffness of the torsional spring has to be increased. However, higher stiffness of the spring leads to lower angular displacement in the mirror oscillation for the same input power. In order to increase the angular displacement the torque applied to the magnet needs to be increased, thus increasing power consumptions. Since the angular displacement can also be improved by increasing the number of turns on the coil while maintaining a constant current, a multilayer coil is used in the study. However, even with these approaches the angular displacement created may not enough to achieve the targeted angular displacement.

Many researchers improved the angular displacement while maintaining the CFF by implementing the compliant structure in the scanner design. Compliant structure is a mechanism designed to transfer the actuating motion to the mirror, such as flexure hinge, lateral spring, cantilever spring and torsional spring [14], [19]. Xiang et al [2] developed a fast laser scanner driven by amplified piezoelectric actuators and flexure hinge was used in the design. However the angular displacement obtained is only 24 mrad. He et al. [20] developed a laser scanner with a permanent magnetic suspension and spherical hinges, the output displacement achieve is only 7o. They did not investigate the effect of magnet position on the scanner characteristics. Kang et al. [21] presented a scanner composed of leaf spring-based double compound linear spring flexure guide mechanisms actuated by voice coil motor (VCM). Sequential quadratic programming (SQP) method was used for design optimization. However, the effect of magnet position on the scanner characteristics was not studied.

In this study, another approach is introduced to achieve a larger angular displacement while meeting the other requirements of the scanner (natural frequency and stress level). Increasing the distance of the magnets from the twist axis of the suspended plate will result in a larger torque and thus angular displacement. This is an economic alternative as it involves only component placement and no modification to the component used in the scanner. However, a system with larger distance from twist axis, as shown in Fig. 2, will suffer in a decrease in the torsional mode frequency, which is a crucial criterion for the torsional scanner design, since the critical flicker frequency (CFF) must be achieved. The selection of the magnet position will require a compromise between the various design parameters.

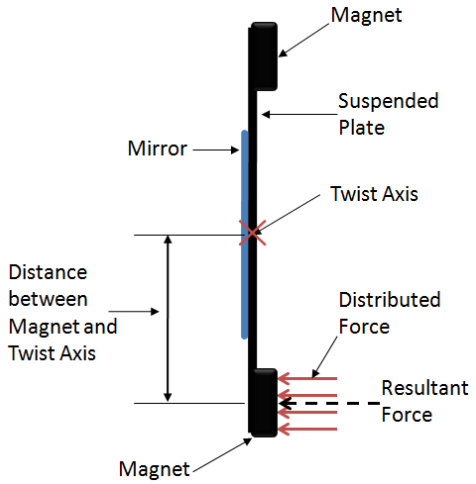

Fig. 2 Schematic of suspended plate (plan view)

II. Analysis and Design

A. Analysis of the Relationship between Magnet Positions and the Natural Frequency

The plate and mirror are suspended by a torsional spring made of commercially available high carbon, thermally treated, flat spring steel of length, and rectangular cross sections as shown in Fig. 3. Table I lists the important properties of the spring material and the dimensions of stock used in this study. Other constraints in the assembly are related to the product performance (resonant frequency), overall size, and component selection.

The torsional spring is assumed to have a uniform cross-sectional area and is made of homogenous isotropic material. It was further assumed that the torsional spring is not loaded beyond the elastic limit. The free vibration was created when the torsional spring is deflected from its equilibrium position through an angle, θ as shown in Fig. 3, its ensuing motion in the absence of any imposed external forces. The existence of damping forces tends to diminish the amplitude of motion with time. Common damping forces include structural

damping, fluid damping and others [22].

TABLE I
PROPERTIES AND DIMENSIONAL CONSTRAINTS

Spring material	1095 steel
Spring shape	Rectangular
Torsional mode	1st
Resonant Frequency	≥CFF
Thickness	0.17-0.2mm
Length	50-80mm
Width	2.5-15mm

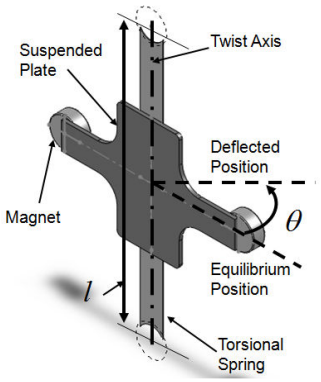

Fig. 3 Twist axis, displacement angle θ, and length l of the torsional spring

In this study, the effect of damping characteristic is assumed to be constant and linear. A restoring moment is generated when the suspended plate is displaced to right, so the spring force acts to the left and vice versa. The moment induced on the suspended plate is proportional to, however it acts in the opposite direction. The relationship between the angular displacement and the restoring moment can be expressed by the general equation [22],

$$I\ddot{\theta} = -k_r\theta - c\dot{\theta} \tag{1}$$

where
k_r is torsional stiffness (N m/rad)
I is mass moment of inertia of the system (kg m^2)
$\ddot{\theta}$ is angular acceleration (rad/s^2)
c is damping coefficient (N m s/rad)

Since $\zeta = \dfrac{c}{2I\omega_n}$ and $\omega_n^{\,2} = \dfrac{k_r}{I}$, then substituting these in the (1), we have

$$\ddot{\theta} + 2\zeta\omega_n\dot{\theta} + \omega_n^{\,2}\theta = 0 \tag{2}$$

where
ω_n is natural circular frequency of the system (rad/s)
ζ is damping ratio

The oscillation of the mass subjected to a restoring moment as described by (2) is called damped free vibration. This oscillation is recognized to be an under-damped vibration as shown in Fig. 4 since the motion undergoes a high numbers of oscillation cycles about the mean (0°) before decaying to zero motion.

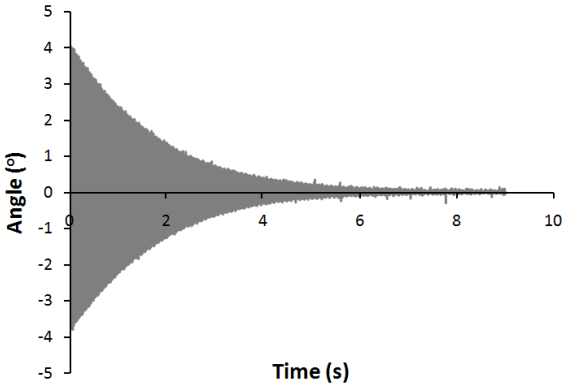

Fig. 4 Angular displacement versus time for free vibration motion of the system

One can anticipate an oscillatory motion for this system, i.e. a solution that gives θ as a periodic function of time. Thus, the function of θ can be expressed by the general equation [22],

$$\theta = \left\{ A_1 e^{i\sqrt{1-\zeta^2}\,\omega_n t} + A_2 e^{-i\sqrt{1-\zeta^2}\,\omega_n t} \right\} e^{-\zeta\omega_n t} \tag{3}$$

where $i = \sqrt{-1}$. The damped angular natural frequency ω_d is introduced in the calculation as the oscillation is under-damped free vibration [22],

$$\omega_d = \omega_n\sqrt{1-\zeta^2} \tag{4}$$

Using Euler formula $e^{\pm i\omega_n t} = \cos\omega_n t \pm i\sin\omega_n t$, (3) can be written as

$$\begin{aligned}\theta &= \left\{ A_1(\cos\omega_d t + i\sin\omega_d t) + A_2(\cos\omega_d t - i\sin\omega_d t) \right\} e^{-\zeta\omega_n t} \\ &= \left\{ (A_1 + A_2)\cos\omega_d t + (A_1 - A_2)i\sin\omega_d t \right\} e^{-\zeta\omega_n t} \\ &= \left\{ A_3\cos\omega_d t + A_4\sin\omega_d t \right\} e^{-\zeta\omega_n t}\end{aligned} \tag{5}$$

where $A_3 = (A_1 + A_2)$ and $A_4 = i(A_1 - A_2)$. Equation (5) shows that the oscillation consists of two harmonics, and can be replaced by a single trigonometric function that includes phase angle ψ, i.e.,

$$\theta = \left\{ C\sin(\omega_d t + \psi) \right\} e^{-\zeta\omega_n t} \tag{6}$$

Equation (6) presents an exponentially decreasing harmonic function, as shown in Fig. 5.

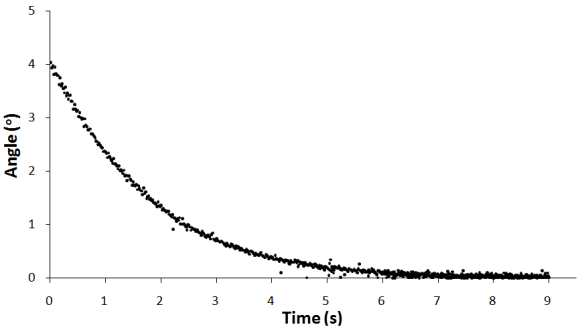

Fig. 5 Maximum positive value of angular displacement versus time for free vibration motion of the system

The damped period is related to angular natural frequency by,

$$\tau_d = 2\pi \frac{1}{\omega_d} \tag{7}$$

Substituting $\omega_n^2 = \frac{k_r}{I}$ into (4), and the frequency f_d of the system is determined to be,

$$f_d = \frac{1}{2\pi}\sqrt{\frac{k_r}{I}\left(1-\zeta^2\right)} \tag{8}$$

The torsional stiffness k_r of the torsional spring can be determined from the following equation [23],

$$k_r = \frac{GK}{l} \tag{9}$$

where
K is a factor that dependents on the form and dimensions of the cross section
l is the length of the spring
G is modulus of rigidity

According to Young [23], the value of K can be estimated from the following approximation,

$$K = ab^3\left[\frac{16}{3} - 3.36\frac{b}{a}\left(1-\frac{b^4}{12a^4}\right)\right] \quad \text{for } a \geq b \tag{10}$$

where
a is half of the width of spring
b is half of the thickness of spring

The mass moment of inertia I needs to be determined according to the cross section of the suspended plate as shown in Fig. 6. The suspended plate can be divided into three rectangular partitions of masses m_{sp^1}, m_{sp^2} and m_{sp^3} as shown in Fig. 6 (b). Both m_{sp^2} and m_{sp^3} are at distance d_2 from the twist axis. The torsional spring is attached at the back of suspended plate and is located on the twist axis with mass of m_{ts} while a magnet is located at each end of suspended plate at distance d_1 from the twist axis of masses m_m. The effect of the small radii at corners of the suspended plate was ignored for this study since the length is much larger than the radii.

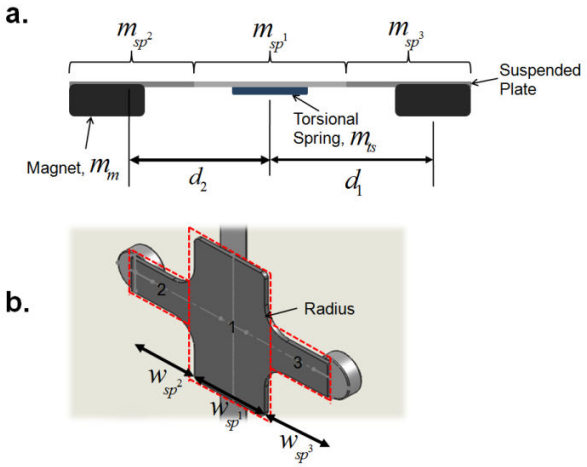

Fig. 6 Suspended plate and magnets, the width and the mass for the component of the scanner: (a) Top view (b) Isometric view

According to the parallel-axis theorem for mass moment of inertia, to determine the mass moment of inertia for the shape such as the suspended plate, the mass moment of inertia of each partition, I', needs to be calculated from[24], [25],

$$I' = \bar{I} + md^2 \tag{11}$$

where
d is perpendicular distance of the centroidal axis of partitions to the twist axis

Then the resultant I of the system is the sum of I' from each partition, i.e.

$$I = 2m_m\left(\frac{1}{4}R^2 + \frac{L^2}{3} + d_1^2\right) + m_{sp^3}\left(\frac{1}{12}h^2 + \frac{1}{12}w_{sp^3}^2 + d_2^2\right) + m_{sp^2}\left(\frac{1}{12}h^2 + \frac{1}{12}w_{sp^2}^2 + d_2^2\right) + m_{sp^1}\left(\frac{1}{12}h^2 + \frac{1}{12}w_{sp^1}^2\right) + m_{ts}\left(\frac{1}{12}t^2 + \frac{1}{12}w^2\right) \tag{12}$$

where
R is radius of magnet
L is length of magnet
$w_{sp^1 \diamond 2 \diamond 3}$ is the width of suspended plate on part1, 2 and 3 as shown in Fig. 6
h is the thickness of suspended plate
t is the thickness of torsional spring
w is the width of torsional spring

Referring to (8), there is an inversely proportional relationship between the frequency of the system and the mass moment of inertia. The CFF depends on the ambient

illumination level and the brightness of the illuminated objects. When viewing objects under bright ambient conditions, the CFF may be as high as 100 Hz. In the dark, however, the CFF is typically around 40 Hz [11]-[13]. Thus the magnet position, *d* in (11) should be adjusted to obtain the targeted frequency which is higher than 40 Hz (CFF). At the same time, the spring dimension (width) needs to be adjusted to give a desired frequency for a given magnet positions as discussed in Section IV *B*.

B. Suspended Plate and Magnet Design

The material properties of the suspended plate and the magnet used in the system are shown in Table II. The size of the envelop for components (suspended plate, torsional spring and mirror) shown in Fig. 1 are 85 mm × 50 mm × 10 mm (L × W × T). The weight of the combined suspended plate, torsional spring and mirror is 6.50 g.

TABLE II
PROPERTIES OF MAGNET AND SUSPENDED PLATE

Magnet material	Neodymium Boron
Magnet dimension (Diameter × Thickness)	7mm×3mm
Suspended Plate material	Galvanized Steel
Galvanized plate young modulus	200GPa
Thickness	0.5 Mm

III. METHODOLOGY

A. Finite Element Analysis (FEA)

A geometric study of the torsional spring was previously performed by varying the thickness, length, and width subject to the following constraints: one of the spring dimension was held constant, while another was allowed to vary and the third dimension was set such that the spring-mass system achieved the target resonance frequency [14]. The maximum stress value of various spring designs were taken as the measure of relative quality of the design.

The spring dimensions were varied over a certain range from the nominal dimension to investigate the sensitivity of the maximum stress to the various dimensions. For instance, the thickness was held constant while the spring width was varied by ±1 mm and the spring length was varied as a dependent variable to achieve the resonant frequency of 44±1 Hz, thus exceeding the minimum CFF (40 Hz). This process was repeated with the width as an independent variable, while the thickness was the dependent variable and length was fixed at a constant value.

Previously, the optimized torsional spring dimensions were determined to be 80 mm× 3.94 mm× 0.17 mm (L × W × T) with a maximum stress of 0.632 GPa and resonant frequency of 43.5 Hz. The results produced the optimized geometry based on the torsional spring without considering the effects of various magnet positions on the characteristics of the scanner. The magnet position used in previous study was held constant at position 1 (Fig. 7).

Since the objective of this study is to select a magnet position that can fulfill the scanner's requirements. Several magnet positions were simulated via FEA, and the effects of magnet position on the scanner's characteristics were investigated. As mentioned before, the position selected for the placement of magnet should give the minimum torsional stress, large angular displacement (30^o), and attain a natural frequency of more than 40 Hz. For each position, a pair of magnets was located on the suspended plate at one of the three possible distances from the twist axis as shown in Fig. 7. Position 1 was selected to be 21.5 mm from the axis due to a size constraint of the scanner since the width of the components were constrainted to be within 50 mm.

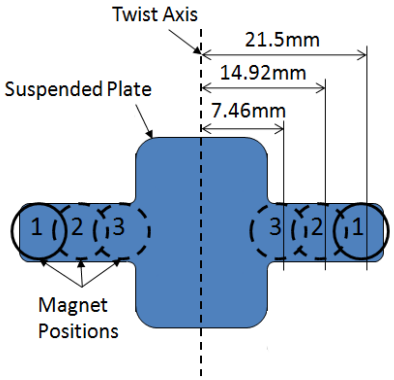

Fig. 7 Positions of magnets on the suspended plate

Two separate analyses (FEA) were carried out to investigate the effect of various magnet positions on the stress level and resonance frequency. The initial simulation was carried out on magnet positions 2 and 3 to determine the effect on the scanner's characteristics since the stress and the resonance frequency of the position 1 had been determined in previous study [14]. The dimensions of the torsional spring and force acting on the magnet were maintained consistent with the previous study carried out at position 1 where the optimized torsional spring dimensions were determined to be 80 mm× 3.94 mm× 0.17 mm (L × W × T) [14]. For position 1, the force acting on the magnet was enough to create angular displacement of 30^o. However, when the same forces were used for position 2 and 3, the variation on angular displacement was created.

Another analysis was performed to understand the relationship between the stress levels as a function of magnet position while allowing the width to change to maintain a constant frequency (44±1 Hz). Initially the length (80mm) and thickness (0.17mm) of the previously optimized torsional spring were held constant [14]. The width of the spring was allowed to change to achieve the targeted resonant frequency, as the width has the dominant effect on the scanner's resonant frequency. According to membrane analogy [23], this phenomenon occurs when the width is larger than thickness (W>>T). The force acting on the magnet is adjusted to maintain an angular displacement of about 30^o for each magnet position. Finally, the maximum stress of the torsional spring was obtained for each magnet position. The initial analysis served as a guide for the effects of magnet position on scanner characteristics (natural frequency, angular

displacement and stress) with similar spring geometries. The second analysis was used to select the magnet position that can fulfill the scanner requirements.

B. Experimental-Simulation Validation

To obtain the natural frequency of the system for experimental-simulation validation, the original spring dimensions of 80.42 mm × 5.5 mm × 0.17 mm($L \times W \times T$) were used. The natural frequency was obtained by applying a small deflection (approximately 4^o) on the suspended plate and releasing it thus creating a free vibration of the system. Fig. 8 shows a schematic diagram of the experimental setup. Measurement of the angular displacement of the plate was performed using the signal from a photodiode sensor connected to a Data Acquisition System (DAQ) for recording. Fig. 9 shows the free oscillation of the suspended plate for magnet position 1 with a period of 0.024 s giving a frequency 41.7 Hz. Comparison between the experimental results and simulation results is shown in Fig. 10.

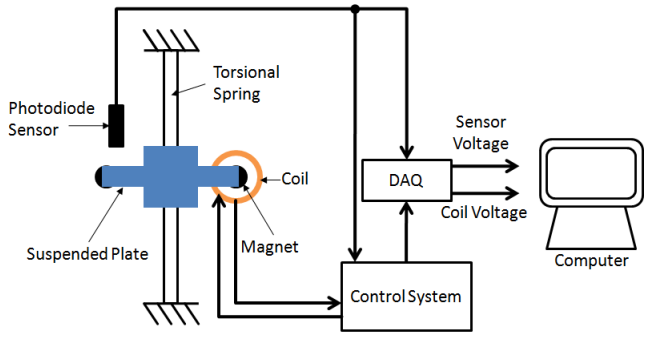

Fig. 8 Experimental setup

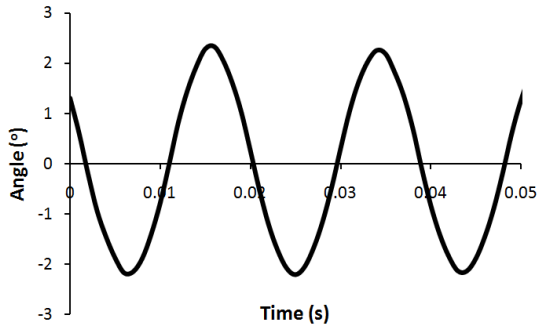

Fig. 9 Angular displacement versus time

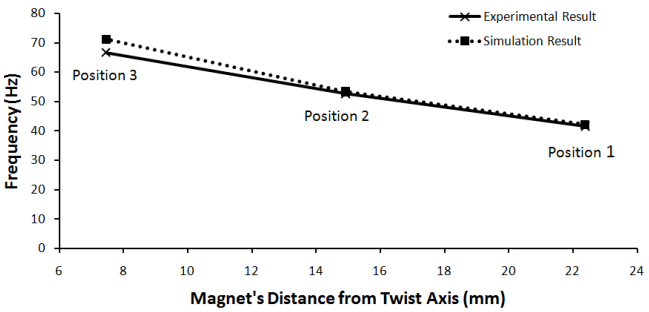

Fig. 10 Variation of natural frequency of the scanner with distance of the magnet from the twist axis

The simulation results of the same dimensions with magnet position 1 (Fig. 10) gave a resonant frequency of 42.2 Hz, while the experimental result is 41.7 Hz, i.e. 1.37% difference. The average difference for the three positions in resonant frequency is 3.18% and is considered acceptably small. Thus, the simulation results are valid for used as a guide to select the magnet position that can fulfill the scanner characteristics. The Fig. 11 shows the FEA model for the torsional spring where the static forces are placed at the magnet to create angular displacement.

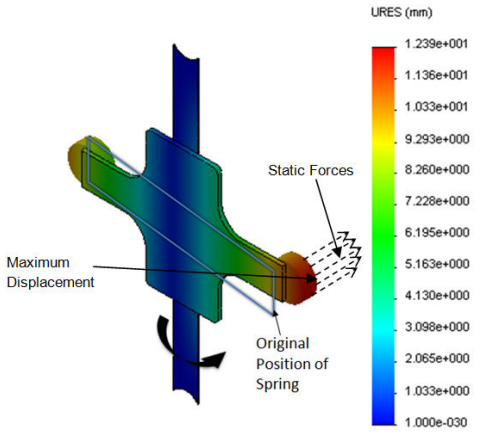

Fig. 11 Displacement distribution of original torsional spring

IV. Results and Discussion

A. Initial Finite Element Analysis

Figs. 12-14 show the results of the initial analysis. The variation of the natural frequency and angular displacement were normalized to the results obtained from position 1 in the simulation study which have ω_0=43.46 *Hz* and $\theta_0 = 29.54^o$.

B. Effect of Various Magnet Positions on the Natural Frequency

The adjustment of placement of magnet from position 1 to position 3 caused an increase in scanner's natural frequency ratio ω/ω_0 from 1 to 1.68 (i.e. 43.46 *Hz* to 73.01 *Hz*) as shown in Fig 12. This phenomenon occurs as the perpendicular distance d from the centroid axis of magnets to the twist axis of suspended plate decreased, thus I became smaller, and the scanner's natural frequency increased simultaneously as can be verified in (8). This marked improvement of the scanner's natural frequency is desirable for eliminating the flickering effect of the scanning image. However, as the magnets are moved closer to the axis of oscillation the resonant frequency increases, which will result in a greater number of stress reversals per unit time, thus resulting in a shorter life expectancy for a given stress level[26].

Fig. 12 ω/ω_0 versus distance from the axis

C. Effect of Magnet Position on Angular Displacement

When the static force $F_t$is imposed to the magnet in position 2 and 3 is similar to the force imposed on magnet in position 1 in the previous study [14], the angular displacements varied from those found in position 1. Moving of magnet from position 1 to position 3 caused a decrease in angular displacement from ratio θ/θ_0 =1 to 0.31 as shown in Fig. 13. This phenomenon can be explained using mathematical model as follows [27].

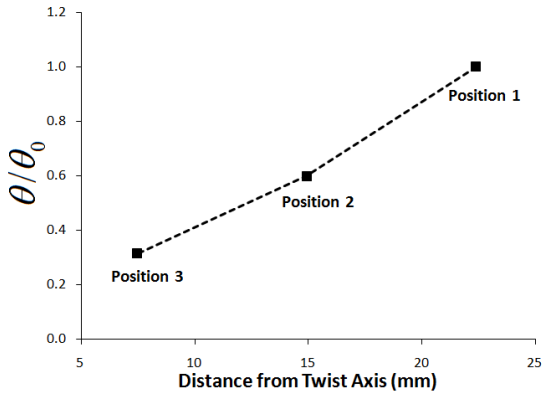

Fig. 13 θ/θ_0 versus distance from the axis

It can be noticed that when the suspended plate with mirror is loaded by the static torque $M_t$and deflected to certain angular displacement ofθ, the relationship between them is given by,

$$\theta = \frac{M_t}{2k_r} \tag{13}$$

$$M_t = F_t d \tag{14}$$

At resonant frequency, the angular displacement of the suspended plate is larger than the static angular displacement by a factor of Q, termed as the "Q factor", then,

$$\theta = \frac{QM_t}{2k_r} \tag{15}$$

where the Q-factor is a measure of the severity of the vibration [22].

Since the static torque M_t is proportional to the perpendicular distance from the centroidal axis d of the suspended plate as shown in (14), it can be noticed that as d increases M_t will increase proportionally. Additionally, the dynamic angular displacement changes accordingly with the change of static torque $M_t$as can be verified in (15). To maintain the targeted angular displacement of 30°, a higher current (approximately 3 times higher) is required at position 3.

D. Effect of Magnet Position on Stress Level

The final consideration is the effects of magnet position on the maximum stress level. One of the objectives for FEA is to obtain a torsional spring that is capable of providing a reasonable life span while maintaining the required frequency and angular displacement. Fig. 14 shows that the stress level decreases as the magnet is moved from position 1 to position 3, nearer to the twist axis. This is because the force acting on the magnets was held constant resulting in smaller angular displacement for positions 2 and 3 as aforementioned. This situation happened for all variations of the torsional spring geometry.

The data in Fig. 14 indicates that the optimized spring should have a maximum length, minimum thickness and minimum width to attain the lowest stress level. According to theory in Mesmacque [28], as long as the repeated loading results in a stress level of less than half of the ultimate stress of the material, the design should have an infinite life. Since the material used is 1095 steel with the ultimate stress of 1.27 GPa, theoretically the torsional spring should have a maximum stress level below 0.635G Pa to ensure an infinite lifespan.

To this point, the discussion has concentrated on the preliminary effects of magnet position on resonance frequency, angular displacement and stress level without altering the applied force. Additionally, the trends of variation on the scanner characteristic (resonance frequency, angular displacement and stress level) were investigated on various magnet positions. Further analysis is required to select the magnet position that can provide the targeted angular displacement while simultaneously modifying the spring geometry to maintain the minimum frequency requirement.

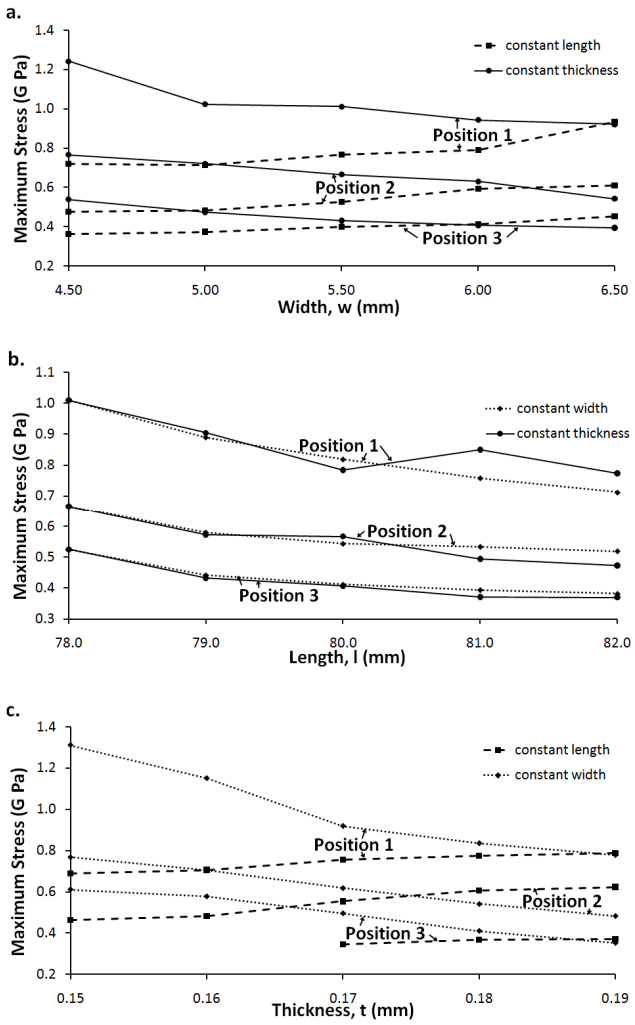

Fig. 14 Maximum stress at different magnet positions for various spring width, length, and thickness

E. Finite Element Analysis for Design Optimization

Fig. 15 shows the results of the second FEA. The width of the torsional spring is allowed to vary to attain the targeted resonant frequency while other dimensions are held constant in analysis. According to the previous study [14], as the width decreases a lower resonant frequency should be obtained. However, as the magnet positions shifts nearer to the twist axis it compensates for the decrease in width and provides an increase of resonant frequency as shown in the initial FEA. This analysis showed that the new torsional spring should have smaller width with the dimensions of 80mm × 2.10mm × 0.17 mm ($L \times W \times T$) giving a resonant frequency of 43.9 Hz with the magnet at position 3. Theoretically, if position 3 is selected, the scanner should fulfill the requirements. However the placements of the magnets in close proximity (position 3) on the suspended plate will affect the magnetic field of the coil to the magnet and, hence the magnetic force that acts on the magnet.

In order to confirm the effect of the placement of the magnets in close proximity to the magnetic field, a pair of magnets were aligned with the same polarity at defined distances on a given plane and tested with the Magnetic Field Viewer Film (MFVF). The resulting magnetic field is shown in Fig. 16 using Magnetic Field Viewer Film. As the magnets are moved closer to the twist axis or nearer to each other, the magnetic fields tend to repel and thus interrupt the interactions of the magnetic field with the air-core coil. The magnetic field around the magnets was simulated by FEA software known as Vector Field Opera-13 as shown in Figs. 17 (a) and (b). Fig. 17 (a) shows that as the magnets move near to each other, the magnetic field tends to merge. While Fig. 17 (b) shows that the magnetic fields tend to isolate when they are moved apart. To minimize the interaction between the magnets, the magnet position 3 cannot be selected in this study although the study shows that the reduction of distance between the magnets and twist axis is needed to attain the targeted natural frequency.

Based on the results of initial and second FEA, the optimized torsional spring is selected to be of dimensions 80mm × 3.94mm × 0.17 mm ($L \times W \times T$) with the resonant frequency of 43.5 Hz, resulting in a maximum stress level of 0.632 GPa. The position 1 is selected since it is able to fulfill the requirements of stress level and frequency while giving the highest displacement for a given coil current. Position 2 will give lower stress levels, however to maintain the targeted angular displacement, higher coil driving current is needed. Position 3 theoretically gives the lowest stress level, but, as has been shown, the magnetic fields tend to destructively interfere with one another, which will result in a further increase of coil driving current.

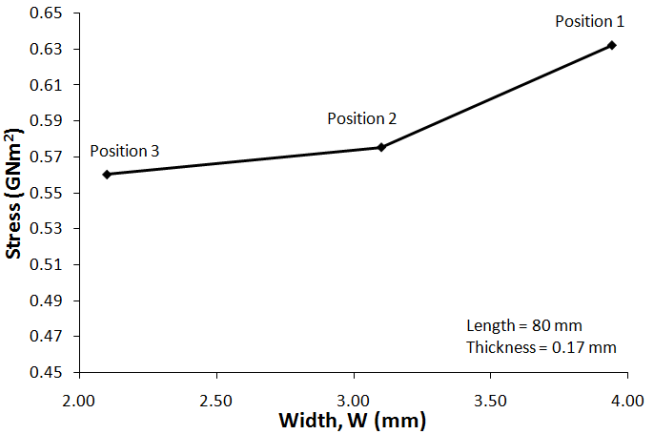

Fig. 15 Stress versus various width for targeted frequency and angular displacement of 30°

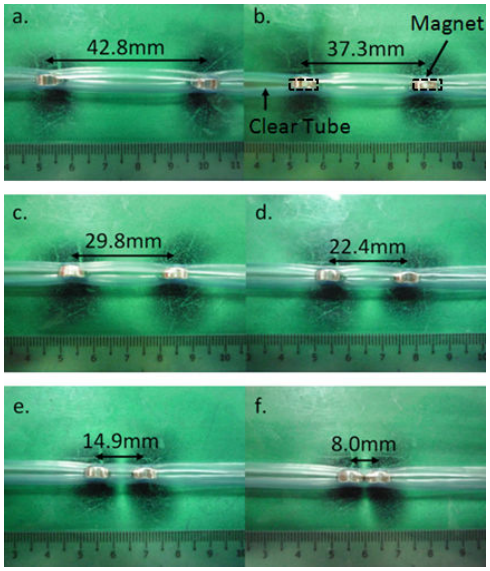

Fig. 16 Magnetic fields as imaged with MFVF

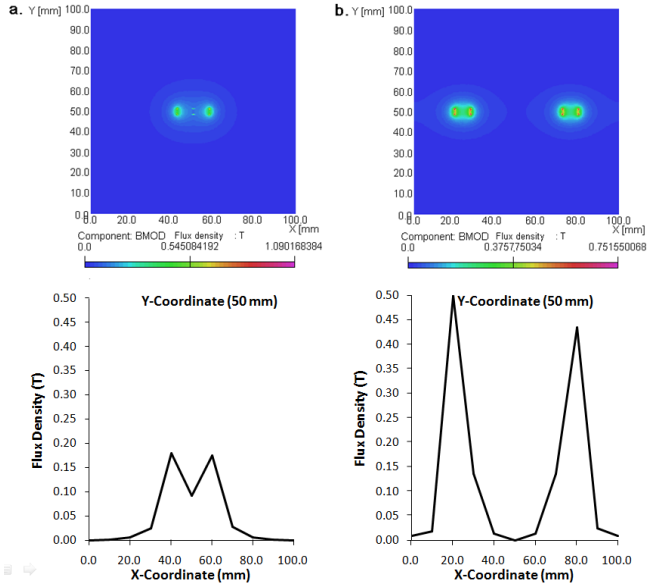

Fig. 17 (a) Magnetic field among two magnets when they are side by side to each other (b) Magnetic field among two magnets when they are apart from each other

V. Conclusions

The magnet positions were analyzed using FEA modeling to study the scanner characteristics. The simulation results agreed with the experiment resonant frequency to within average value 3.18%. Therefore, the simulated results were used as a guide in selecting the magnet position that can achieve the targeted angular displacement and CFF. The initial analysis indicates that when the magnets are placed closer to the twist axis, lower stress levels and angular displacement were obtained with higher resonance frequency. Thus, the trends of the scanner characteristics (resonance frequency, angular displacement and stress level) varied with magnet positions were investigated in initial FEA. Theoretically, the magnets should be nearer (position 3) for material cost reduction since a shorter suspended plate can be used. However, magnetic field interruption occurred when they placed in close proximity. Thus, position 1 was selected for the placement of magnets since this position can provide the desired scanner characteristics. With the optimized torsional spring and the position selected (position 1), the maximum stress of 0.632 GPa was found on the spring. Therefore, the scanner should exhibits reasonable lifetimes under ideal conditions, which is in agreement with theory. This position will also result in the lowest overall energy consumption, and thus it was selected for the placement of magnets.

Acknowledgment

The work was financially supported by The Vice-Chancellor's Award of UniversitiSains Malaysia.

References

[1] Dao P., and Dentamaro A., 2003, "Development of a Deployable Aerosol / Water Vapor Lidar to Characterize the Atmosphere," Proc. SPIE, 5087(781).
[2] Xiang S., Chen S., Wu X., Xiao D., and Zheng X., 2010, "Study on Fast Linear Scanning for a New Laser Scanner," Opt. Laser Technol., 42(1), pp. 42-46.
[3] Grupp M., Seefeld T., and Vollertsen F., 2003, "Laser Beam Welding with Scanner," Proc. Second International WLT, Munich, pp. 1-5.
[4] Urey H., 2002, "Torsional MEMS Scanner Design for High-Resolution Display Systems," Proc. SPIE, 4773(July), pp. 27-37.
[5] Qingkun Z., Ben-Tzvi P., Dapeng F., and Goldenberg A. A., 2008, "Design of Fast Steering Mirror Systems for Precision Laser Beams Steering," 2008 IEEE International Workshop on Robotic and Sensors Environments, (October), pp. 144-149.
[6] Cochran R. W., and Vassar R. H., 1990, "Fast-Steering Mirrors in Optical Control Systems," Proc. SPIE, 1303, pp. 245-251.
[7] Burgert O., Treichel T., Dressler C., and Gessat M., 2010, "Storing Data Generated by Optical Surface Scanners Using DICOM- A Work Item Proposal," Proc. SPIE, 7628, p. 76280D-76280D-10.
[8] Zhou J., Yin H., and Wang Y., 2009, "Research on the Structure and Dynamic Characteristics of a Fast-Steering Mirror," Proc. SPIE, 7281, p. 72810J-72810J-5.
[9] Aylward R. P., 2003, "Advanced Galvanometer-Based Optical Scanner Design," Sensor Review, 23(3), pp. 216–222.
[10] Hii K.-fu, Vallance R. R., and Mengüc M. P., 2010, "Design , Operation , and Motion Characteristics of a Precise Piezoelectric Linear Motor," Precision Engineering, 34, pp. 231-241.
[11] Mason P., Hill M., and Ses- G., 1981, "Piezoelectricity , Its History and Applications," Journal of Acoustical Society of America, 70(6), pp. 1561-1566.
[12] Remy M., Lemarquand G., Castagnede B., Guyader G., and Renault T., 2008, "Ironless and Leakage Free Voice-Coil Motor Made of Bonded Magnets," IEEE Transactions on Magnetics, 44(11), pp. 4289-4292.
[13] Jung K. S., and Baek Y. S., 2002, "Development of a Novel Maglev Positioner with Self-Stabilizing Property," Mechatronics, 12, pp. 771-790.
[14] Koay L. K., and Gitano-Briggs H., 2011, "Design and Optimization of Mechanically Resonant Torsional Spring Mechanism for Laser Light Dispersion Applications," ASME J Mech. Des., 133(1), p. 014504.
[15] Park J., Lee S., and Kwak B. M., 2012, "Design Optimization of Piezoelectric Energy Harvester Subject to Tip Excitation," Journal of Mechanical Science and Technology, 26(1), pp. 137-143.
[16] Kheng L. B., Kean K. L., and Gitano-Briggs H., 2010, "Design Optimization and Fatigue Testing of an Electronically-Driven Mechanically-Resonant Cantilever Spring Mechanism," Int. J. Mater. Des., 31(8), pp. 4023-4028.
[17] Greenwood V. J., Smith E. L., Goldsmith A. R., Cuthill I. C., Crisp L. H., Walter-swan M. B., and Bennett A. T. D., 2004, "Does the Flicker Frequency of Fluorescent Lighting Affect the Welfare of Captive

European Starlings□?," Applied Animal Behaviour Science, 86, pp. 145-159.
[18] Becker C., and Elliott M. A., 2006, "Flicker-Induced Color and Form□: Interdependencies and Relation to Stimulation Frequency and Phase," Consciousness and Cognition, 15, pp. 175-196.
[19] Todd B., Jensen B. D., Schultz S. M., and Hawkins A. R., 2010, "Design and Testing of a Thin-Flexure Bistable Mechanism," Journal of Mechanical Design, 132(July), pp. 1-7.
[20] He N., Jia W., and Huang L., 2006, "Design and Mechanism Analysis of a Novel Type Compact Single Mirror Laser Scanner," Sensors And Actuators, 125, pp. 482-485.
[21] Kang D., Kim K., Kim D., Shim J., Gweon D.-G., and Jeong J., 2009, "Optimal Design of High Precision XY-Scanner with Nanometer-Level Resolution and Millimeter-Level Working Range," Mechatronics, 19(4), pp. 562-570.
[22] Balachandran B., and Magrab E. B., 2004, Vibrations, Belment: Thomson Learning.
[23] Young W. C., and Budynas R. G., 2002, Roark's Formulas for Stress and Strain, McGraw-Hill, New York.
[24] P. Beer F., and Russell, E. J., 1985, Mechanics for Engineers-Dynamics, McGraw-Hill, United States of America.
[25] Cheng F.-H., 1997, Statics and Strength of Materials, McGraw-Hill, New York.
[26] Scott-emuakpor O., Shen M. H., and Cross C. J., 2007, "Development of an Improved High Cycle Fatigue Criterion," Journal of Engineering for Gas Turbines and Power, 129(January), pp. 162-169.
[27] Asada N., Takeuchi M., Vaganov V., and Belov N., 2000, "Silicon Micro-Optical Scanner," Sensors and Actuators A: Physical, 83(1-3), pp. 284–290.
[28] Mesmacque G., and Farfa S., 2004, "High Cycle Fatigue , Low Cycle Fatigue and Failure Modes of a Carburized Steel," International Journal of Fatigue, 26, pp. 673-678.